Model-Driven Reconstruction of 3-D Buildings Using LiDAR Data

Yuanfan Zheng and Qihao Weng, *Member, IEEE*

***Abstract*—Data-driven and model-driven strategies are two basic approaches for building reconstruction based on LiDAR data. Due to the data noise and limitations in existing algorithms, the data-driven approach can neither construct a complete roof plane nor construct irregular planes. This letter proposes a model-driven approach to reconstruct 3-D building structures by developing prototypical roofs for commercial and residential buildings. The experiment was conducted in the City of Indianapolis, IN, USA, using the LiDAR data and building footprints provided by the city government. Irregular building footprints were first decomposed into nonintersecting and mostly quadrangular blocks for the identification of the most probable prototypical roofs. A decision tree classifier was applied to classify all building footprints into seven subtypes based on the physical and morphological parameters of buildings. The modeling of prototypical roofs was finished with the parameters including the length, the width, and the orientation of the principal axis of each building block that were computed from the LiDAR data using the static moment equations. Additional parameters, including the mean height, the top height, and the gutter height, were also considered as needed for some subtypes. Complex roofs were reconstructed by assembling adjacent prototypical roofs. The decision tree classification method was finally applied to 268 building blocks and achieved an overall accuracy of 82.1% for seven classes. A 3-D geographic information system building database that includes commercial and residential buildings in two chosen city blocks was created for further applications. This letter created a more completed building roof structure than the existing data-driven approach and demonstrated the reliability of a decision tree classifier in categorizing building roofs.**

***Index Terms*—Building database, building reconstruction, LiDAR, model-driven approach, 3-D geographic information system (GIS).**

I. Introduction

TWO-dimensional building footprints are often available at the national level for developed countries. However, compared with 2-D building footprints, 3-D city models are rarely available, but they are valuable in more applications in urban planning, environmental planning, particularly solar radiation calculations or noise emission simulation [1], and urban structure analysis since they contain more physical and morphological information for an individual building. The availability of laser scanning techniques makes the acquisition of the height information of ground features easier and more accurate. The automated generation of 3-D city models can be achieved by using the 2-D building footprints and LiDAR data as input.

The general building modeling procedure includes two major steps, i.e., the detection of building boundaries and the reconstruction of building models (see [2] and [3]). In the past decades, numerous approaches for the detection and reconstruction of building boundaries are from high-resolution aerial imagery [4], LiDAR data [1], and multiple data sources [5]. They separated buildings from other features based on a series of hypotheses. Since the previous methods have developed well the methods for detecting building boundaries, we focused on the reconstruction part in this letter. Data-driven and model-driven approaches are the two basic strategies for building reconstruction. For the data-driven strategies, buildings are considered representing the aggregation of roof planes represented by the blocks of point clouds or the digital surface model (DSM). The roof planes are determined by segmenting the completed point cloud into different parts, applying methods such as edge-based methods [6], region growing [7], random sample consensus (RANSAC) [8], clustering [9], or the combination of two or more algorithms [10]. However, each method has its own limitations. The edge-based methods are susceptible to outliers and incomplete edges, whereas the region growing methods are subject to seed selection and usually fails in smooth transition between two planes. The RANSAC methods often lead to an unneeded false plane, and the clustering technique needs to define the number of classes and the cluster center subjectively. A common limitation of the data-driven approaches is that the modeling results may be affected by data noise. They cannot construct a complete roof plane or irregular planes.

In contrast to data-driven strategies, model-driven strategies employ parametric building models, which are stored in a predefined library, to reconstruct the blocks of point clouds or the DSM. The model-driven methods have several advantages. First, in roof primitives, the constraints of member facets are predefined and ensure regularized or completed reconstructions. Moreover, the combination of a few primitives is much simpler than the organization of a bunch of facets [11]. The works in [12] and [13] both presented a method that reconstructed buildings from a DSM. Essentially, the 2-D building footprints were first decomposed manually or automatically. The 3-D blocks were then placed on the 2-D supports using a Gibbs model that controlled both the block assemblage and the fitting to the data. A Bayesian decision found the best fit roof primitives in the predefined library to represent the given blocks of point clouds using a Markov Chain Monte Carlo

Manuscript received October 11, 2014; revised February 7, 2015; accepted March 3, 2015.

The authors are with the Center for Urban and Environmental Change, Department of Earth and Environmental Systems, Indiana State University, Terre Haute, IN 47809 USA (e-mail: qihao.weng@indstate.edu).

Color versions of one or more of the figures in this paper are available online at http://ieeexplore.ieee.org.

Digital Object Identifier 10.1109/LGRS.2015.2412535

sampler associated with original proposition kernels. The work in [14] reconstructed building roofs based on the directions of each extracted ridge line fitted from the local maxima of the pixels using RANSAC. However, these methods cannot perform a quantitative accuracy assessment of the modeling results. Henn *et al.* [1] approached model selection using supervised classification, which achieved a classification accuracy of 95%. However, it was restricted to only five types of roof primitives. Many commonly seen roofs, such as half-hipped roofs or connectors, including cross-gable roofs and intersecting roofs, were not included.

In this letter, we added the commonly seen half-hipped roofs, cross-gable roofs, and intersecting roofs to the building library. A decision tree classifier was applied to classify the DSM within the building footprints into different types of roofs based on a hierarchical structure, which would be beneficial for the roof reconstruction. The objective of this letter is to present a model-driven approach to reconstruct 3-D buildings for a large urban area, including both commercial and residential buildings based on a LiDAR DSM and building footprint data sets.

Fig. 1. Subset of the two test sites in the City of Indianapolis.

II. Methodology

A. Study Area and Data

Two data sources were used, i.e., LiDAR data and building footprint polygons, including size, energy consumption, and ownership information. In the USA, LiDAR data are available nationwide. One of the most famous public data inventories is the U.S. Interagency Elevation Inventory, which is a collaborative effort of the National Oceanic and Atmospheric Administration and the U.S. Geological Survey, and it is updated annually. Building footprints are available in almost all major cities, which are typically stored as geographic information system (GIS) shapefiles.

The study area included two city blocks, which were located in the City of Indianapolis. Each of them covered about 0.25 km^2 of urban settlement. Fig. 1 presents the subset of these two test sites. They were characterized by commercial buildings and residential houses with different roof shapes. Some roofs were overlapped by adjacent trees. The last-pulse LiDAR DSM and the digital elevation model (DEM) with a spatial resolution of 0.91 m were acquired during the year of 2009. These LIDAR data had a vertical accuracy of 0.31 ft (9.45 cm) at the 95% confidence level by the National Standard for Spatial Data Accuracy testing procedure. The LiDAR normal height model (NHM), which represented the absolute height information of the feature objects above the ground surface, was calculated as follows:

$$\mathrm{NHM} = \mathrm{DSM} - \mathrm{DEM}. \tag{1}$$

Building footprints were used to mask out the nonbuilding features, such as tall trees in the LiDAR NHM.

B. Definition of Structured Roof Types

A roof model can be seen as an aggregation of planar meshes with a well-defined structure [1]. Building roofs are

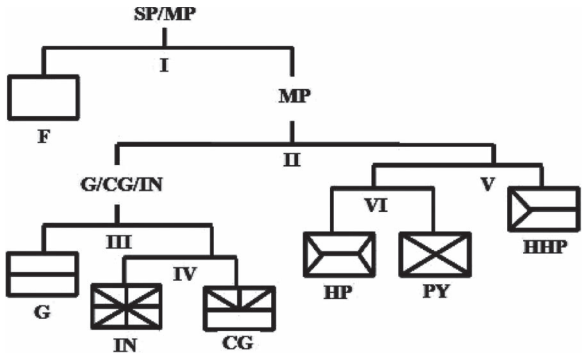

Fig. 2. Hierarchy for the classification of roof models (SP: single plane; MP: multiple plane; F: flat; G: gable; CG: cross gable; IN: intersecting; HP: hipped; HHP: half-hipped; PY: pyramid).

distinguished into simple and complex roofs. For simple roofs, the model-driven strategies searched for the most appropriate model among the basic building models in the model library [1]. Relatively complex buildings can be decomposed into nonintersecting and mostly quadrangular segments, and they are assembled later to form the entire building [11]. In this letter, seven types of roofs were observed in the study area (see Fig. 2). A flat roof is a subtype of a roof with a single roof plane. A gable roof can be defined as a roof that has two upward sloping sides that meet each other at the ridge, which is also the top of the roof. In the case of cross-gable roofs, there is one more gable at either side of the upward plane. The intersecting roofs, on the other hand, have gables on both sides of the original upward planes. A hipped roof is a type of roof where all sides slope upward to the ridge but usually with a much more gentle slope compared with a gable roof. Half-hipped roofs and pyramidal roofs are both special cases of the hipped roof. Half-hipped roofs only have a single hip on one

TABLE I
STATISTICS RESULTS OF THE PARAMETERS FOR EACH ROOF CLASS (F: FLAT; G: GABLE; CG: CROSS GABLE; IN: INTERSECTING; HP: HIPPED; HHP: HALF-HIPPED; PY: PYRAMID)

	Mean Slope (feet)	Mean Aspect (degree)	Moran's I
F	12.6-29.8	120.4-250.1	0.11-0.32
G	27.4-49.9	107-230.9	0.23-0.61
CG	26.3-42.7	116.2-222	0.45-0.66
IN	31.4-49	150.3-200.8	0.30-0.63
HP	29.7-44.1	131.5-197.1	0.51-0.79
HHP	26.3-56.9	79.3-234.4	0.48-0.74
PY	29.6-46.6	131.6-189	0.44-0.72

side. Pyramidal roofs can be seen as hipped roofs with a ridge length of 0.

C. Classification of Building Roofs

The presence of seven roof types results in a multiclassification problem. Methods should be developed to simplify the multiclassification to a binary classification. It can be observed that the geometry shape of different roof models has a hierarchical structure (see Fig. 2). Therefore, a hierarchical-based classification method should be considered. A decision tree classifier was applied to classify the building NHM into seven types of roofs. First, it performed multistage classifications by using a series of binary decisions to separate one class from others. A different set of rules was applied to the binary classification in each step, which can also handle the data with different scales and ranges. The decision tree classifier has not been used to estimate roof types in the context of building roof reconstruction in such a way.

Training data for all types of roofs were collected to calculate certain parameters, which included the mean slope, the mean aspect, and Moran's I index for each class, as shown in Table I. The first step was the discrimination of the roof models based on the number of roof planes (Step I in Fig. 2). A constraint combined the threshold of the mean slope, and Moran's I index was used to separate the flat roof from the others. For further binary classification in the following steps, additional parameters were considered. Each building footprint has two axes that intersect in the geometric center (see Fig. 3). The principal axis has to be determined for gable, cross-gable, hipped, and half-hipped roofs first, which can be defined as an axis parallel to the roof ridge. In this letter, the standard deviations of the pixel heights located in two axes were calculated separately. The axis with a lower standard deviation was defined as the principal axis, i.e., Axis A in Fig. 3. The distance from two roof edges to Axis A is equal. It was assumed that the pixels in the gable, cross-gable, and intersecting roofs had a lower standard deviation on a line, which is located in the middle of the building footprint and is parallel to the roof ridge, as compared with those of the pyramid, hipped, and half-hipped roofs. Therefore, in Step II, a binary classification can be performed based on the following rule: if a coefficient of variation $Cv(a)$ was lower than a predefined threshold, the building footprint could be classified as a gable, cross-gable, or intersecting roof; otherwise it could be classified as a pyramid, hipped, or half-hipped roof. The coefficient of variation $Cv(a)$ can be calculated as

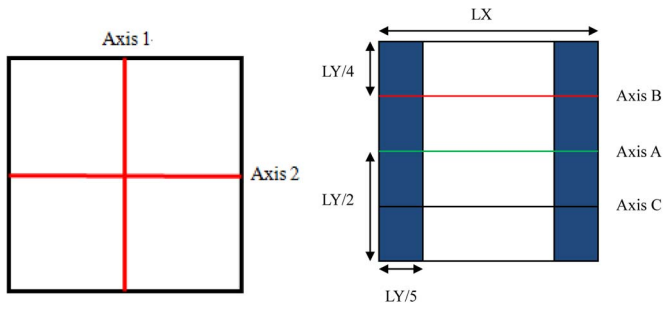

Fig. 3. (Left panel) Building footprint with two axes that intersect in the geometric center. (Right panel) Three axes (Axes A, B, and C) and two masks (the blue region).

$$Cv(a) = \frac{\sigma(a)}{\mu(a)}. \tag{2}$$

It measures the extent of height variability in Axis A, where $\sigma(a)$ is the height standard deviation of the pixels located in Axis A, which is the principal axis (see Fig. 3), and $\mu(a)$ is the mean height of the pixels intersecting with Axis A. The discrimination among the gable, cross-gable, and intersecting roofs in Steps III and IV was performed based on the consideration of two additional parameters $Cv(b)$ and $Cv(c)$. They can be calculated using the following equations:

$$Cv(b) = \frac{\sigma(b)}{\mu(b)} \tag{3}$$

$$Cv(c) = \frac{\sigma(c)}{\mu(c)}. \tag{4}$$

The distance from Axis B or C to Axis A and that between two roof edges are equal (see Fig. 3). $Cv(a)$, $Cv(b)$, and $Cv(c)$ generally measure the extent of height variability in Axes A, B, and C, respectively. If both $Cv(b)$ and $Cv(c)$ were lower than a threshold, the building footprint would be classified as a gable roof, as gable roofs only had a single plane on each side, and the pixels located in Axes B and C should have a lower standard deviation. If $Cv(b)$ or $Cv(c)$ was lower than a threshold, the building footprint would be classified as a cross-gable roof, as it had an intersection of gables on one side of the ridge. If neither $Cv(b)$ nor $Cv(c)$ was lower than a threshold, the building footprint would be classified as an intersecting roof.

The classification between half-hipped roofs and hipped roofs or pyramid roofs was executed in Step V (see Fig. 2), which is based on the symmetry of their shapes. Two masked areas of the rectangles, which were close to the gutter of the roof, were chosen, and the mask width was proportional to the rectangle width by a factor of 1/5 (see Fig. 3). If the number of selected pixels in each mask area was noted as N, then the mean of the pixel values, which was ranked above 0.3 N by increasing the order, was computed for two masked areas as $H1$ and $H2$ to avoid the data noise. If the difference between $H1$ and $H2$ was larger than a threshold, the given building footprint would be classified as half-hipped roofs, as they were

TABLE II
RULES USED IN EACH CLASSIFICATION STEP (F: FLAT; G: GABLE; CG: CROSS GABLE; IN: INTERSECTING; HP: HIPPED; HHP: HALF-HIPPED; PY: PYRAMID)

Step	Feature	Rules
I	F	Mean Slope ranges from 12.6-29.8 and Moran's I index ranges from 0.11-0.32
II	G	Cv(a) <= 0.109
III	CG	Cv(b) <= 0.118 and Cv(c) <= 0.118
IV	IN	Cv(b) > 0.118 and Cv(c) > 0.118
V	HHP	H1-H2 >= 9.43
VI	HP	Cv(a) <= 0.154

not as symmetrical as the hipped roofs and the pyramid roofs. An additional rule was set up to classify the hipped roofs and the pyramid roofs in the final step. If the coefficient of variation $Cv(a)$ was lower than a predefined threshold, the building footprint would be classified as a hipped roof; otherwise, it would be classified as a pyramid roof. The constraints used in each classification step were listed in Table II. The thresholds were determined based on the calculated statistics of the training samples.

D. Three-Dimensional Building Reconstruction

The 3-D building roofs were reconstructed by applying the prototypical roofs to represent buildings, as described in the previous step. Parameters such as the length, the width, and the orientation of the principal axis were needed for all types of buildings. Length L_x and width L_y can be calculated from the following:

$$L\_x = N/R^*P \qquad L\_y = N/C^*P \tag{5}$$

where N is the number of pixels included in a given building footprint, R is the number of rows, C is the number of columns, and P is the pixel size. The orientation of the principal axis was calculated by using the method provided in [15]. The application of the static moment equations on the pixels within the given building footprint allowed the calculation of its gravity center as follows:

$$\mu X = \frac{(\sum_{i=1}^{n} Xi)}{n} \qquad \mu Y = \frac{(\sum_{i=1}^{n})}{n} \tag{6}$$

where μX and μY are the abscissas and ordinates in the original coordinate system OXY, respectively, and n is the number of pixels included in the given building footprint. The orientation of the principal axis Θ could be calculated by using

$$\Theta = \frac{1}{2}\arctan\frac{2\sum_{i=1}^{n}(Xi-\mu X)(Yi-\mu Y)}{\sum_{i=1}^{n}(Xi-\mu X)^2-\sum_{i=1}^{n}(Yi-\mu Y)^2}. \tag{7}$$

Additional parameters were required to model the prototypical roofs. For a flat roof, the mean height of all pixels was the only parameter needed for calculation. However, for the rest of the subtypes, the top (ridge) height and the gutter height were required, which were estimated by using the method proposed in [16]. Masks were separately defined to include the chosen pixels for the gutter height and top height estimation. A parameter N was used to define the number of selected pixels, and the mean of the pixel values, which were ranked in an increasing order between 0.25 N and 0.75 N, was computed for the gutter and top heights in different mask areas. The ridge was assumed to be located in the middle of a given quadrangular building block, splitting it into two equal parts. Complex roofs were reconstructed by assembling adjacent prototypical roofs.

TABLE III
CLASSIFICATION RESULT FOR EACH ROOF CLASS (F: FLAT; G: GABLE; CG: CROSS GABLE; IN: INTERSECTING; HP: HIPPED; HHP: HALF-HIPPED; PY: PYRAMID) WITH AN OVERALL CLASSIFICATION ACCURACY OF 82.09% AND A KAPPA COEFFICIENT OF 0.77

	Reference total count	Map total count	Number of correct	Producer's accuracy (PA)%	User's accuracy (UA)%
F	47	54	47	100.00%	87.03%
G	106	90	85	80.19%	94.44%
CG	40	42	34	85.00%	80.95%
IN	20	23	15	75.00%	65.22%
HP	16	24	11	68.75%	45.83%
HHP	28	24	22	78.57%	91.67%
PY	11	11	6	54.55%	54.55%

III. RESULTS

The decision tree classification was finally applied to 268 building blocks and achieved an overall accuracy of 82.1% for seven classes (see Table III). It is found that flat roofs can be successfully separated from others, except for gable roofs, by using the threshold of the mean slope and Moran's I index. The classification among gable roofs, cross-gable roofs, and intersecting roofs worked well too. Only a small number of gable roofs with big dormers were classified as cross-gable roofs. Some gable roofs were misclassified as hipped roofs, which was probably due to the fact that some building roofs were not symmetrical since the endpoints located on different sides of the ridge can still have a large difference in height. Some hipped roofs were grouped as intersecting roofs, which may be due to the fact that a high value of the standard deviation can be found on the planes located in both sides of the ridge. Many pyramid roofs were confused with hipped roofs since the only difference was the length of the ridge (a pyramid roof can be seen as a special hipped roof with a ridge length of 0). Overall, the decision tree classifier was demonstrated to have the ability to classify building roofs into subtypes.

The prototypical roofs were finally applied to building blocks based on the roof classification result. The model of the prototypical roofs was built in the Google SketchUp software with the knowledge of parameters including the length, the width, the orientation of the principal axis, the top height, and the gutter height of each building block, which were derived from the original LiDAR DEM. Complex roofs with multiple types of prototypical roofs were reconstructed by assembling adjacent building blocks together. A 3-D GIS building database, which included commercial and residential buildings in the two chosen city blocks, was created for further application. Fig. 4 presents the subset of the reconstruction result from the study areas in the city of Indianapolis, IN, USA, visualized in ArcScene.

Fig. 4. Subsets of the reconstruction result from the study areas in the City of Indianapolis, IN, USA, visualized in ArcScene.

IV. Conclusion

This letter has developed a more complete building roof structure than the existing data-driven methods and has demonstrated the reliability of a decision tree classifier in categorizing building roofs. It has provided a method for building roof reconstruction and identification, which is solely based on LiDAR and building footprints. The decision tree classification achieved an overall accuracy of 82.1% and a Kappa index of 0.77 for separating seven classes based on the differences among their physical and morphological parameters estimated from the training data. Therefore, the prototypical roofs created based on some chosen parameters (the length, the width, the orientation of the principal axis, the mean height, the top height, and the gutter height) calculated from the LiDAR data can be applied. The reconstruction of complex buildings using the model-driven approach was proven to be reliable since irregular footprints can be decomposed into multiple quadrangular blocks and assembled after the prototype roofs were identified.

A limitation in this letter lay in its use of simplified prototypical roofs, which were created based on some assumptions. Such assumptions included ridges that are always located in the center position, the uniform height of the gutter, and the exclusion of substructures or dormers. Further improvements can be achieved by the combination of a data-driven approach with a model-driven approach. Although the data-driven approach usually produces irregular and incomplete roof planes, it involved many algorithms and techniques to delineate roof features, such as substructures, ridges, step edges, antennas, and dormers. It is particularly useful if high-spatial-resolution imagery and dense LiDAR data are used. Additional parameters obtained from a data-driven approach, such as the ridge location, the ridge length, the height difference, and the distance of the substructure position to each edge, can be added to increase the accuracy of the building roof classification and the 3-D building reconstruction. Finally, our primitive library only included seven prototypes since we only chose two city blocks as the study area with 268 building blocks. In order to apply this method to larger urban areas with more prototypes, new physical and morphological parameters such as the height difference, the height variation, and a convex area may be necessary to identify more complicated roofs such as stadia, churches, or some irregular architectures.

References

[1] A. Henn, G. Groger, V. Stroh, and L. Plumer, "Model driven reconstruction of roofs from sparse LiDAR point clouds," *ISPRS J. Photogramm. Remote Sens.*, vol. 76, pp. 17–29, Feb. 2013.

[2] C. Baillard and H. Maiter, "3-D reconstruction of urban scenes from aerial stereo imagery: A focusing strategy," *Comput. Vis. Image Understanding*, vol. 76, no. 3, pp. 244–258, Dec. 1999.

[3] T. A. Tao, "Parametric reconstruction for complex building from LIDAR and vector maps using a divide-and-conquer strategy," in *Int. Archives Photogramm., Remote Sens. Spatial Inf. Sci.*, Beijing, China, 2008, vol. 37, B3a, pp. 133–138.

[4] M. Cord and D. Declercq, "Bayesian model identification: Application to building reconstruction in aerial imagery," in *Proc. ICP*, Kobe, Japan, Oct. 1999, vol. 3, pp. 140–144.

[5] N. Haala, C. Brenner, and K. H. Anders, "3-D urban GIS from laser altimeter and 2-D map data," *Int. Archives Photogramm. Remote Sens., Remote Sens. Spatial Inf. Sci.*, vol. 32, pp. 339–346, 1998.

[6] X. Y. Jiang and H. Bunke, "Fast segmentation of range images into planar regions by scan line grouping," *Mach. Vis. Appl.*, vol. 7, no. 2, pp. 115–122, Apr. 1994.

[7] A. Alharthy and J. Bethel, "Detailed building reconstruction from airborne laser data using a moving surface method," *Int. Archives Photogramm. Remote Sens.*, vol. 35, pp. 213–218, 2004.

[8] R. Hartley, and A. Zisserman, *Multiple View Geometry in Computer Vision*, 2nd ed. Cambridge, U.K.: Cambridge Univ. Press, 2004, pp. 117–123.

[9] J. Shan and A. Sampath, "Building extraction from LiDAR point clouds based on clustering techniques," *Topographic Laser Ranging and Scanning: Principles and Processing*, J. Shan and C. Toth, Eds. Boca Raton, FL, USA: CRC, 2008, ch. 15, pp. 423–446.

[10] P. Dorninger and N. Pfeifer, "A comprehensive automatic 3D approach for building extraction, reconstruction, and regularization from airborne laser scanning point clouds," *Sensors*, vol. 8, no. 11, pp. 7323–7343, Nov. 2008.

[11] M. Kada and L. Mckinley, "3D building reconstruction from Lidar based on a cell decomposition approach," *Int. Archives Photogramm., Remote Sens. Spatial Inf. Sci.*, vol. 38, pp. 47–52, Sep. 2009.

[12] F. Lafarge, X. Descombes, J. Zerubia, and M. Deseilligny, "Structural approach for building reconstruction from a single DSM," *IEEE Trans. Pattern Anal. Mach. Intell.*, vol. 6, no. 1, pp. 135–147, Jan. 2007.

[13] H. Huang, C. Brenner, and M. Sester, "A generative statistical approach to automatic 3D building roof reconstruction from laser scanning data," *ISPRS J. Photogramm. Remote Sens.*, vol. 79, pp. 29–43, May 2013.

[14] H. Arefi, M. Hahn, and P. Reinartz, "Ridge based decomposition of complex buildings for 3D model generation from high resolution digital surface models," *Proc. ISPRS Istanbul Workshop Modeling Opt. Airborne Spaceborne Sens., WG 1/4, IAPRS*, Oct. 2010, vol. 38-1/W17, pp. 1–7.

[15] F. T. Kurdi, T. Landes, P. Grussenmeyer, and M. Koehl, "Model-driven and data-driven approaches using LiDAR data: Analysis and comparison," *Int. Archives Photogramm., Remote Sens. Spatial Inf. Sci.*, vol. 36, pp. 87–92, Sep. 2007.

[16] F. Lafarge, X. Descombes, J. Zerubia, and M. Deseilligny, "A parametric model for automatic 3D building reconstruction from high resolution satellite images," Inria, Le Chesnay Cedex, France, Res. Rep. RR-5687, 2006, p. 29.